ACS OMEGA

http://pubs.acs.org/journal/acsodf

Article

Research on the Dynamic Model of Fireball Thermal Dose Based on the Effective Band Integral Method

Pan Pei,* Hongmian Du,* and Xiaojian Hao

Cite This: *ACS Omega* 2023, 8, 29717−29724

Read Online

ACCESS | Metrics & More | Article Recommendations

ABSTRACT: In the brief combustion process of an explosive fireball, the fireball can release considerable radiant energy. Aiming at the problem that the Stephen−Boltzmann formula calculates the fireball surface radiant energy (full band), it does not match the working bands of most infrared thermal imagers. So, in this paper, we obtain dynamic parameters such as the temperature, diameter, and height of the fireball from the infrared thermal image of the thermobaric explosive fireball, achieve on-site atmospheric transmittance by the temperature calibration target, and integrate within the effective wavelength band of the infrared thermal imager, and a precise dynamic model of the fireball's thermal radiation dose was finally established. According to the fireball test data of the infrared thermal imaging camera in the 2−5 μm band, the heat dose of the fireball at different distances is calculated, which is about 1/2.5 of the calculation result of the Stephen−Boltzmann full-band integral formula. The calculations in this paper are more accurate than measurements from existing static models and provide a better assessment of the thermal damage performance of various types of munitions.

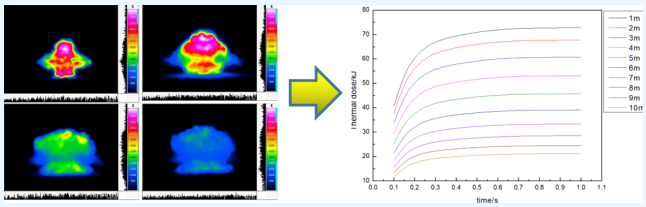

1. INTRODUCTION

The explosion of new munitions forms a huge high-temperature fireball and consumes a large amount of oxygen around it. The violent high temperature and asphyxia effect is significantly higher than that of conventional explosives, which can kill and destroy a certain range of living forces. In addition, sustained high temperatures can also destroy diffuse biological and chemical weapons and avoid secondary injury caused by the leakage of biological and chemical weapons.[1−3]

In the early period, some scholars used static models to calculate the hot dose of fireballs. They ignored the change process of the fireball and simply assumed that the diameter, location, and thermal radiation of the fireball are constant over the full duration of the event, and the results were generally large.[2−10] The parameters of fireball temperature, fireball size, and rising height are all dynamically changed, and the dynamic model of fireball thermal radiation is proposed according to the real change process of the fireball.[11−18]

Further research shows that the dynamic model of fireball thermal radiation still uses an empirical and semiempirical formula to calculate the parameters of fireball, and the calculation of fireball surface radiation energy directly uses the Stephen−Boltzmann formula, which is only applicable to full-band temperature measurement and not applicable to existing thermal imaging cameras.[19] The method of calculating the atmospheric transmission rate is simple to apply the related formulas, ignoring the differences in appearance and environment in different parts of the country, and there is a certain error with the actual atmospheric transmission rate.[20]

To solve the current problems faced by researchers with static model fireball parameters that deviate from actual values and large errors in the assessment of thermal effects destruction, based on calculating the dynamic model of the effects of fireball thermal radiation and based on the fireball image taken by an infrared thermal imager, the dynamic parameters of fireball change over time are obtained by the multiorder fitting method, the radiation theorem of Planck black body is obtained by multiorder fitting method based on this, the Stephen−Boltzmann formula is improved, the energy radiated on the surface of the fireball is obtained by using the effective band integral method in the working band of the infrared thermal imager, and the on-site atmospheric transmission rate is obtained by using the field temperature calibration target. Thus, using the dynamic parameters of fireball measurement, a dynamic model of the hot dose of fireball is established based on the effective band integral method, and the thermal effect of fireball is evaluated.

Received: June 6, 2023
Accepted: July 20, 2023
Published: August 3, 2023

https://doi.org/10.1021/acsomega.3c03980
ACS Omega 2023, 8, 29717−29724

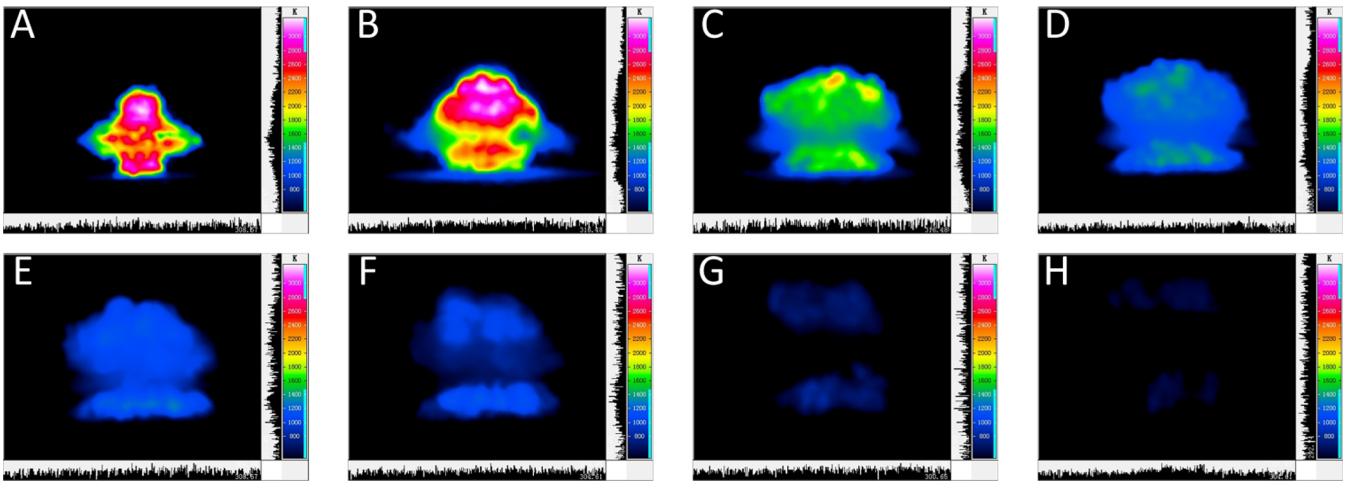

Figure 1. Infrared images of the thermobaric explosive within 875 ms after the explosion: (A) 1 ms, (B) 125 ms, (C) 250 ms, (D) 375 ms, (E) 500 ms, (F) 625 ms, (G) 750 ms, (H) 875 ms.

2. EXPERIMENTAL PROCEDURE

Given the high temperature of the fireball in the explosion field, short response time, harsh measurement environment, and poor repeatability, this article uses the Image5300 high-frame-rate infrared thermal imager produced by Infratec Company, it has a sampling frame rate of 200 Hz. The working band is between 2 and 5 μm, and the temperature measurement range is −40 to 3000 °C, the temperature measurement accuracy can reach 0.015 K, and the dynamic data of each stage of the fireball's formation, ascending, spreading, and disappearance can be obtained. The infrared thermal imager completely records the explosion process of the thermo-pressure explosive simulated warhead. By inputting the fireball emissivity and atmospheric transmittance parameters, it can effectively reverse the temperature field of the explosive fireball. The test was conducted on land with an open field of view, the site temperature was 26.9 °C, the air humidity was 76.6%, and the site distance measured was 77.8 m. The maximum temperature of the 30 kg thermobaric explosive fireball during the entire explosion was 3386.12 K, the maximum diameter was 23.14 m, and the maximum height of the center of the fireball was 7.98 m. Figure 1 shows a typical infrared image during a period after the explosion of the 30 kg thermobaric explosive.

Distinguished by the process of explosion products, the fireball from the explosion to dissipation is divided into three stages: (1) Radiation expansion stage. Due to the temperature pressure bomb violent redox reaction and the formation of a very-high-temperature fireball, the fireball is everywhere to form an isothermal radiation front. At the same time, the shock wave compresses the surrounding air to form a wavefront and begins to propagate outward. The radiation expansion phase lasts for a duration in the order of ms, corresponding to Figure 1A,B. (2) Second stage: Shock wave expansion phase. The shock wavefront coupled with the radiation front and the surface of the fireball shows extreme points of irradiation brightness, where the temperature and pressure munitions and metal additives lead to extremely complex reaction products due to insufficient oxygen content (Figure 1C). Subsequently, with the shock wave out of the fireball radiation front, the fireball irradiance decreases and deflagration generation begins to cover the fireball surface (Figure 1D,E). (3) Third stage: the smoke cloud dissipation phase. As the fireball continues to lose energy, its own temperature will continue to decrease, the brightness gradually decreases, and the fireball in this phase gradually becomes smaller and dissipates (Figure 1F−H).

By observing the infrared image of the fireball within 875 ms of the thermobaric explosion, it is found that the explosive fireball is irregularly elliptical from the beginning of 1 ms, and the red high-temperature area of about 2500 K is mainly distributed in the center of the fireball, and the distribution is not uniform. At 250 ms, the shape of the fireball has changed significantly, the volume has begun to expand, the lower and upper parts of the fireball have become larger, and they have begun to appear as mushroom clouds and have a gradual upward trend. The temperature of the fireball is concentrated at about 1600 K; when the fireball develops to 375 ms, the horizontal diameter of the fireball became smaller and began to change and extend in the vertical direction. The overall temperature of the fireball also changed significantly, and the temperature was around 1000 K.

In addition, the diameter and height parameters of the fireball are also constantly changing. No matter whether it is the growth or dissipation stage of the fireball, the traits of the fireball also change continuously as the explosion occurs. Therefore, for the calculation of fireball parameters, neither empirical nor semiempirical formula[16] is applicable. It is necessary to obtain the data of the fireball parameters over time based on experimental data and then fit the corresponding time-varying curve.

There are many factors that affect the performance of the explosive fireball. Thermobaric explosive is mainly composed of high-energy explosives, high-calorific-value metal aluminum powder, oxidizing agent, blunting agent/adhesive, etc. The temperature of the fireball depends on the combustion characteristics of the high-energy explosive DNTF/HMX, charge density, shape of the charge, experimental environment, and many other factors, so the specific temperature needs to be determined by experimental tests. The height of the fireball H depends on the detonation method of high-energy explosives, charge shape, experimental environment, and many other factors. The diameter of the fireball D depends on the weight of the thermobaric bomb, container size, experimental environment, and many other factors. The height of the fireball H depends on the detonation method of high-energy explosives, charge shape, experimental environment, and other

https://doi.org/10.1021/acsomega.3c03980
ACS Omega 2023, 8, 29717−29724

factors. The diameter of the fireball D depends on the weight of the thermobaric bomb, container size, experimental environment, and other factors. The influence of T/H/D factors is more complex and cannot be established through a simple analysis of the chemical formula function. The specific parameters can only be obtained through experiments.

2.1. Fireball Temperature. We select the maximum temperature T_m in each frame of the image during the fireball explosion and the average temperature of the equivalent thermal radiation intensity[11] Ta and draw the curve of the fireball temperature, as shown in Figure 2.

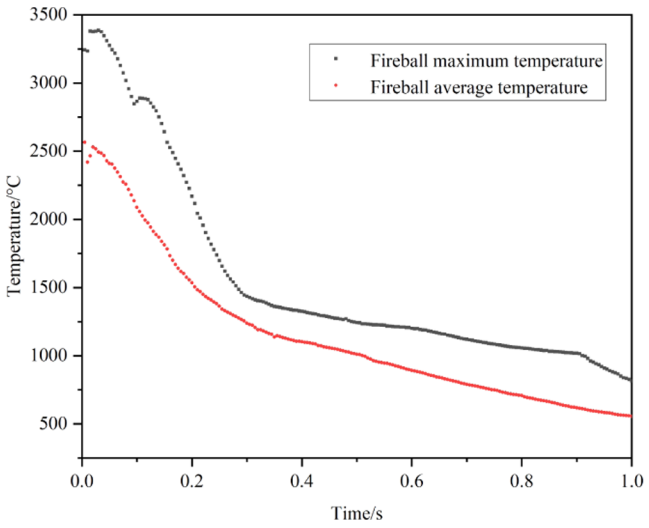

Figure 2. Maximum temperature Tm and the average temperature Ta of the equivalent thermal radiation intensity of a fireball.

After the thermobaric exploded, it was a heterogeneous oxygen-lean combustion process. The temperature distribution at each point on the surface of the fireball was not uniform. The temperature of most areas on the surface of the exploded fireball was less than the maximum temperature Tm at that moment, so the single point of each frame of the image was the maximum temperature and does not represent the overall temperature of the entire surface of the fireball. And the highest point temperature on the surface of the fireball cannot be used directly to calculate the overall radiant energy on the surface of the fireball. According to the principle of radiation temperature measurement, it is more reasonable to use the average temperature parameter of the fireball surface, that is, the average temperature Ta of the equivalent thermal radiation intensity, as the temperature of the fireball surface.[11] We uniformly select 50 points within the effective area of the flame; n is 50 and i starts from 1.

$$T_a = \sqrt[4]{\sum_i^n \frac{T_i^4}{n}} \tag{1}$$

2.2. Fireball Diameter and Height. The experimental site length calibration is used to obtain the fireball diameter D that is shown in Figure 3. The actual height of the marker in the figure is 4.48 m, and the corresponding pixel L in the infrared image is 48 pix. The experimental site length calibration factor is 0.0933 m/pix. Taking the maximum diameter of the fireball as an example, the number of pixels in the horizontal direction is 248 pix, multiplied by the

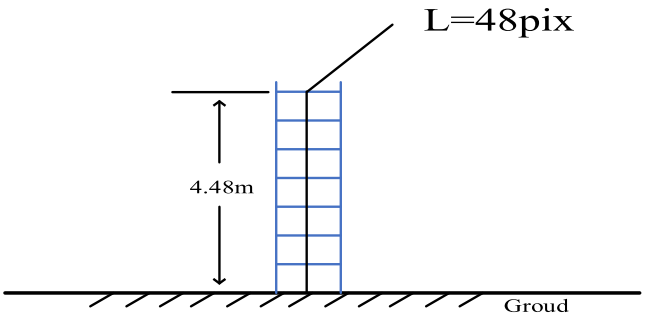

Figure 3. Experimental site length calibration schematic.

experimental field length calibration factor is 0.0933 m/pix, so the maximum diameter of the fireball is 23.14 m.

When the fireball center off-ground height H data extraction is carried out, the fireball off-ground height data H is obtained according to the above-mentioned field calibration method. A fireball image with the label "Ground" marked the ground horizontal line, as a height zero, recording the height difference of the center of the fireball from the ground, combined with the scale of the field calibration, to determine the height of the center of the fireball off the ground, to obtain all of the fireball center off-ground height data H.

2.3. Multiorder Fitting of Fireball Parameters. Through the postprocessing of the fireball data, the statistical data of the maximum temperature Tm of the fireball surface, the average temperature Ta of the equivalent thermal radiation intensity, the diameter D of the fireball, and the height H from the ground of the center of the fireball are obtained. The coefficient of determination R^2 calculated by the order fitting equation is used as the evaluation standard. Detailed fitting of each parameter, including the coefficient of determination of R^2 values is shown in Table 1. The calculation results show that the coefficient of determination R^2 of each parameter fitting equation is the best when the 6-order fitting is used, all of which are above 0.95, with high fitting accuracy compared to other lower fitting orders. Figure 4 also shows the dynamic parameters curve comparison chart before and after fitting of the explosive fireball (Table 2).

3. ESTABLISHING A DYNAMIC MODEL OF FIREBALL THERMAL DOSE Q

After the ammunition explodes, the high-temperature fireball continuously emits heat radiation. And the heat flux $q(x,t)$ received by the target at a certain distance is the thermal radiation energy $E(t)$ on the surface of the fireball, the view factor $F(x, t)$, and the atmospheric transmittance $\tau_a(x, t)$ constitute a function. Then, we can obtain the thermal radiation dynamic model of the fireball.[12]

$$q(x, t) = E(t)F(x, t)\tau_a(x, t) \tag{2}$$

The fireball lasts so short that the heat received by the target is too late to be lost. Therefore, the thermal dose criterion is used to evaluate the damaging effect on the exposed target, that is, the heat flux $q(x,t)$ in the fireball integrates within the duration t to obtain the dynamic model of the fireball thermal dose Q.

$$Q = \int_0^t E(t)F(x, t)\tau_a(x, t)\mathrm{d}t \tag{3}$$

3.1. Effective Band Method for Calculating the Radiation Energy of the Surface of the Fireball. The

https://doi.org/10.1021/acsomega.3c03980
ACS Omega 2023, 8, 29717−29724

Table 1. Comparison of Multiorder Fitted Coefficients of Determination (R^2)

	1st-order(R^2)	2nd-order(R^2)	3rd-order(R^2)	4th-order(R^2)	5th-order(R^2)	6th-order(R^2)
Tm	0.7357	0.9330	0.9796	0.9803	0.9889	0.9960
Ta	0.8459	0.9631	0.9923	0.9950	0.9959	0.9984
D	0.8457	0.8505	0.8819	0.8907	0.9471	0.9557
H	0.9282	0.9282	0.9540	0.9544	0.9567	0.9727

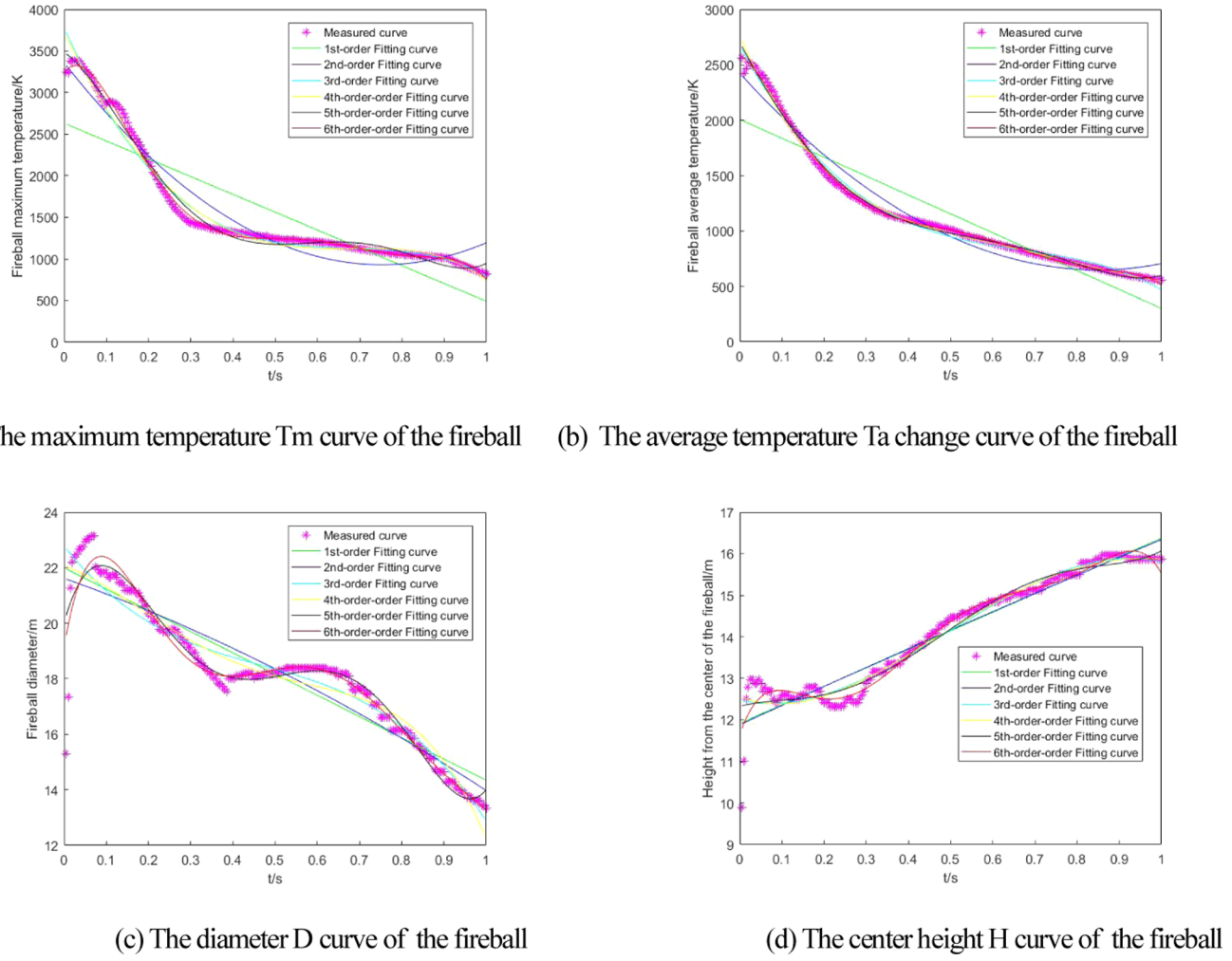

Figure 4. Contrast curve diagram of the dynamic parameters of explosive fireball before and after fitting.

Table 2. Fireball 6-Order Fitting Coefficient of Thermobaric Explosive

	$Y = at + bt^2 + ct^3 + dt^4 + et^5 + ft^6 + g$							
Y	a	b	c	d	e	f	g	R^2
Tm/K	6280	-1.309×10^5	5.008×10^5	-8.428×10^5	6.667×10^5	-2.026×10^5	3241	0.996
Ta/K	−2843	-3.623×10^4	1.797×10^5	-3.359×10^5	2.822×10^5	-8.898×10^4	2593	0.998
D/m	89.09	−783.90	2523	−3809	2718	−743.3	19.14	0.956
H/m	14.77	−142.30	570.1	−1035	875.6	−281.6	5.827	0.973

theoretical basis of infrared thermal imager camera radiation temperature measurement is Planck's law of distribution, which reveals the distribution of radiant energy of an object at different temperatures according to wavelength, and its spectral radiant emission degree M_λ is expressed as

$$M_\lambda = \varepsilon C_1 \lambda^{-5} (\exp^{C_2/(\lambda T)} - 1)^{-1} \quad (4)$$

where M_λ is spectral radiant exitance, W·m^{-2}·μm^{-1}; C_1 and C_2 are the first and second radiation constants, respectively, C_1 = 3.7427 × 108 (W·m^{-2}·μm^4) and C_2 = 1.4388 × 104 (μm·K); T is the temperature value of the fireball, K; and ε is the fireball emissivity, and the value measured earlier is 0.43.

The calculation formula of fireball surface radiant energy in the literature[14] regards the fireball surface radiant energy as a fixed value related to fuel quality, combustion heat, and combustion heat radiation coefficient, and does not reflect the strong dependence of surface radiant energy on temperature T. Related studies show that the explosion flame is consistent

https://doi.org/10.1021/acsomega.3c03980
ACS Omega 2023, 8, 29717−29724

with the characteristics of the ash body,[21] and the average temperature based on the equivalent thermal radiation intensity is more consistent with the gray-body radiation theory and better reflects the nature of the thermal radiation on the surface of the fireball. Reference 9 uses the Stephen−Boltzmann formula to integrate Planck radiation formula 4 in the full band from 0 to ∞ and obtains the total radiation of the fireball at temperature T from 0 to ∞

$$E = \int_0^\infty \varepsilon C_1 \lambda^{-5} (\exp^{C_2/(\lambda T)} - 1)^{-1} \, \mathrm{d}\lambda = \varepsilon \sigma T^4 \tag{5}$$

where $\sigma = 5.67 \times 10^{-8} (\mathrm{w \cdot m^{-2} \cdot k^{-4}})$ is the Stephen−Boltzmann constant and E is the thermal radiation energy, $\mathrm{w \cdot m^{-2}}$.

In the current situation, there is no infrared detector that responds to all bands at the same time. Infrared thermal imagers are usually divided into three bands: short wave (1−2.5 μm), medium wave (2−5 μm), and long wave (8−14 μm). But 2−5 and 8−14 μm are two atmospheric windows commonly used in infrared thermal imaging cameras. Within this range, the atmospheric transmission rate is high, with less infrared radiation attenuation.

Most infrared thermometers cannot detect all of the infrared radiation energy in the band from 0 to ∞. An infrared thermal imager usually works in the atmospheric window of the band 2−5 or 8−14 μm,[19] and the infrared detector captures only the fireball radiation energy in this band. Given the current situation, this article proposes an effective band integration method that is suitable for most infrared thermal imaging cameras, that is, integrating in the 2−5 μm or 8−14 μm bands of an infrared thermal imager using the Planck radiation formula 4, to obtain the radiant energy on the surface of the fireball scientifically

$$E(t) = \int_{\lambda_1}^{\lambda_2} \varepsilon C_1 \lambda^{-5} (\exp^{C_2/(\lambda T)} - 1)^{-1} \mathrm{d}\lambda \tag{6}$$

where $E(t)$ is the thermal radiation energy, $\mathrm{w \cdot m^{-2}}$, and from λ_1 to λ_2 are the effective bands of the infrared thermal imager, μm.

Figure 5 is the Planck radiation curve. The curve is integrated from 0 to ∞ get all of the areas under the curve, corresponding to E in Formula 5. The effective band integration method in this article is working in the infrared thermal imager λ_1 integrated into the λ_2 band, which corresponds to $E(t)$ in Formula 6. Through the comparison of the areas in the graph, we can see the fireball radiation energy E calculated by the full band method using Formula 5. The surface radiation energy E is greater than the fireball surface thermal radiation energy $E(t)$ obtained by the effective band integration method used in this article. Therefore, for an infrared thermal imager working in a certain band, the effective band integration method used to calculate the radiant energy on the surface of the fireball is more reasonable.

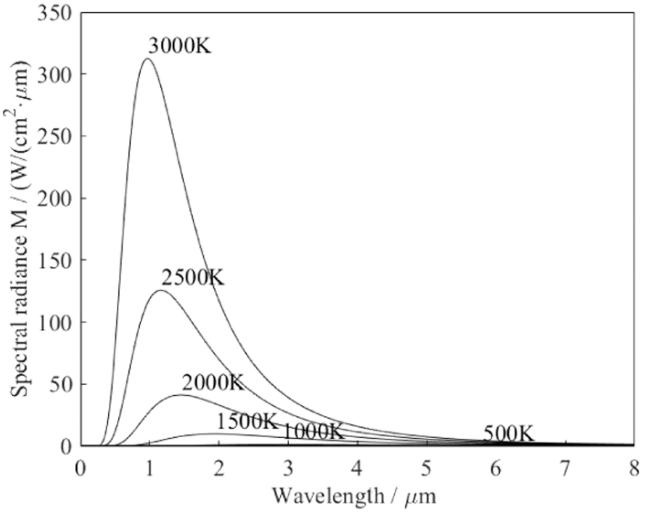

Figure 5. Planck radiation curve.

3.2. View Factor. The target may be in various directions around the fireball, that is, the target cannot receive the radiant energy from every point on the radiating surface, but only a part of it. Therefore, it is necessary to introduce the parameter of the view factor. The view factor is the ratio of the radiant energy received by the target and the radiant energy released by the fireball per unit area.[16]

The target is in a certain position on the ground, and the vertical distance from the center of the fireball is X, m. As shown in Figure 6, the view factors at different distances from the target are

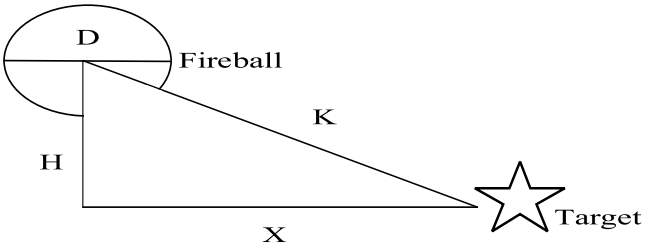

Figure 6. Fireball view factor.

$$F(x, t) = \frac{D_{(t)}^2}{4K_{(t)}^2} \tag{7}$$

$$k(t) = \sqrt{H_{(t)}^2 + X^2} \tag{8}$$

where $D(t)$ is a function of the diameter of the fireball with time, $H(t)$ is a function of the height of the center of the fireball with time, X is the horizontal and vertical distance from the target to the fireball, m, and t is time, s.

3.3. Atmospheric Transmittance. Infrared radiation will be absorbed and scattered by gases such as water vapor and carbon dioxide, which are widely present in the atmosphere, which will eventually lead to the attenuation of thermal radiation. Thermal damage test sites may include deserts, Gobi, coastal plains, and other areas, and the climate and environment vary greatly. The atmospheric transmittance τ_a is an extremely fluctuating physical quantity. When the explosion temperature is measured in the explosion field, it is necessary to accurately combine the local natural environmental conditions to determine the atmospheric transmittance of the scene.

In this paper, using a temperature calibration target, as shown in Figure 7, the infrared thermal imager is calibrated on-site to obtain the correction of the on-site environmental parameters. At this time, the infrared thermal imager measurement model is as follows

$$\mathrm{DN}_t = \alpha \cdot \tau_a \cdot L + \mathrm{DN}_0 \tag{9}$$

https://doi.org/10.1021/acsomega.3c03980
ACS Omega 2023, 8, 29717−29724

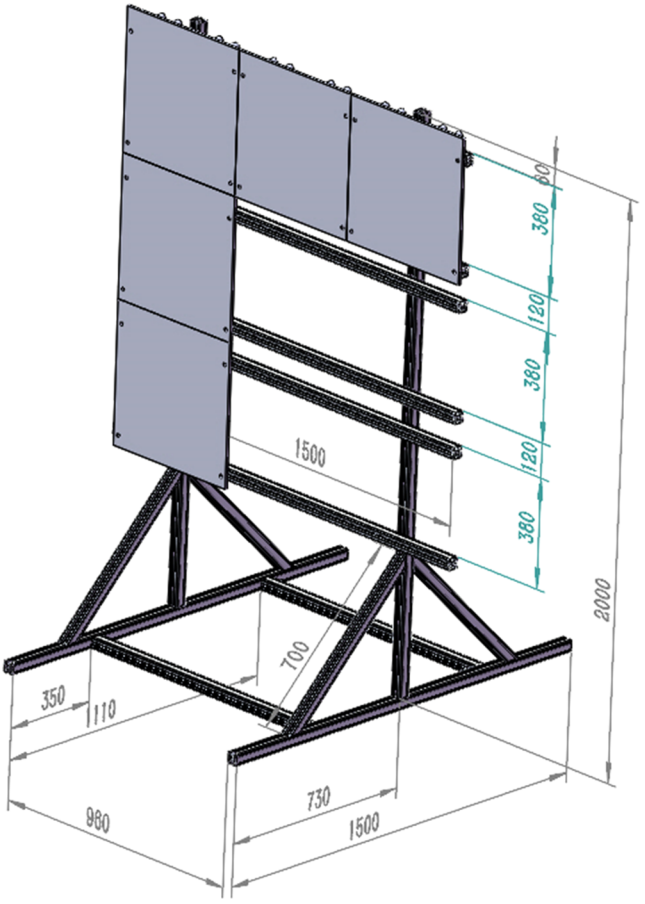

Figure 7. Schematic diagram of the mechanical structure of temperature calibration target.

where DN_t is the digital quantity output by the infrared thermal imager (dimensionless, generally expressed in grayscale), α is the radiance response of the infrared measurement system, τ_a is the on-site atmospheric transmittance, and L is the radiance value. We carry out multi-temperature data collection on-site, perform data fitting, and get the on-site value of α and DN_0.

The temperature calibration target was set at a low working temperature T_L, the radiance of the calibration target is L_L, and the system response value measured by the infrared thermal imager to the calibration target is DN_L. Then, the temperature calibration target was set under the high working temperature T_H, the radiance of the calibration target is L_H, and the system response value measured by the infrared thermal imager to the calibration target is DN_H. According to the measurement values of the low- and high-temperature calibration targets by the infrared thermal imager, the atmospheric transmittance τ_a of the scene can be solved by using the radiation measurement model of eq 9

$$\tau_a = \frac{DN_H - DN_L}{\alpha(L_H - L_L)} \tag{10}$$

In formulas 3 and 6−10, the effective band of the infrared thermal imager is 2−5 μm and the fireball thermal radiation dose Q is obtained according to the effective band integration method. The dynamic expression is

$$Q = \int_0^1 \int_2^5 \varepsilon C_1 \lambda^{-5} (\exp^{C_2/(\lambda T_t)} - 1)^{-1} \times \frac{D_{(t)}^2}{4[H_{(t)}^2 + X^2]} \times \frac{DN_H - DN_L}{\alpha(L_H - L_L)} \, d\lambda dt \tag{11}$$

The thermal radiation heat dose Q_2 of the fireball was calculated using the Stephen−Boltzmann formula of the full-band method

$$Q_2 = \int_0^1 \varepsilon\sigma T^4 \times \frac{D_{(t)}^2}{4[H_{(t)}^2 + X^2]} \times \frac{DN_H - DN_L}{\alpha(L_H - L_L)} \, dt \tag{12}$$

4. RESULTS AND DISCUSSION

The thermal dose Q damage criterion takes the thermal dose received by the target as the criterion of whether the target is destroyed. When the thermal dose received by the target is greater than or equal to the critical thermal dose for target destruction, the target is destroyed. Its scope of application is: the duration of the heat dose acting on the target is so short that the heat received by the target is too late to be lost. It is very suitable for explosive explosions with a short duration, so the Q criterion is selected as the damage criterion in this article.[22] As shown in Table 3.

Table 3. Criteria for Thermal Dose Q Damage

thermal dose/kJ·m^{-2}	damage effect
1030	ignite wood
592	death
392	seriously injured
375	third-degree burns
250	second-degree burns
172	flesh wound
125	first-degree burn
65	skin pain

Table 4. Comparison of Fireball Heat Dose Results at Different Distances

	Q/kJ·m^{-2}		Q_2/kJ·m^{-2}		
distance/(m)	thermal dose	damage effect	thermal dose	damage effect	Q_2/Q
1	72.81	skin pain	184.10	flesh wound	2.53
2	67.79	skin pain	171.29	first-degree burn	2.53
3	60.80	below skin pain	153.51	first-degree burn	2.52
4	53.14	below skin pain	134.05	first-degree burn	2.52
5	45.74	below skin pain	115.27	skin pain	2.52
6	39.09	below skin pain	98.43	skin pain	2.52
7	33.36	below skin pain	83.94	skin pain	2.52
8	28.54	below skin pain	71.76	skin pain	2.51
9	24.52	below skin pain	61.62	below skin pain	2.51
10	21.19	below skin pain	53.23	below skin pain	2.51

https://doi.org/10.1021/acsomega.3c03980
ACS Omega 2023, 8, 29717−29724

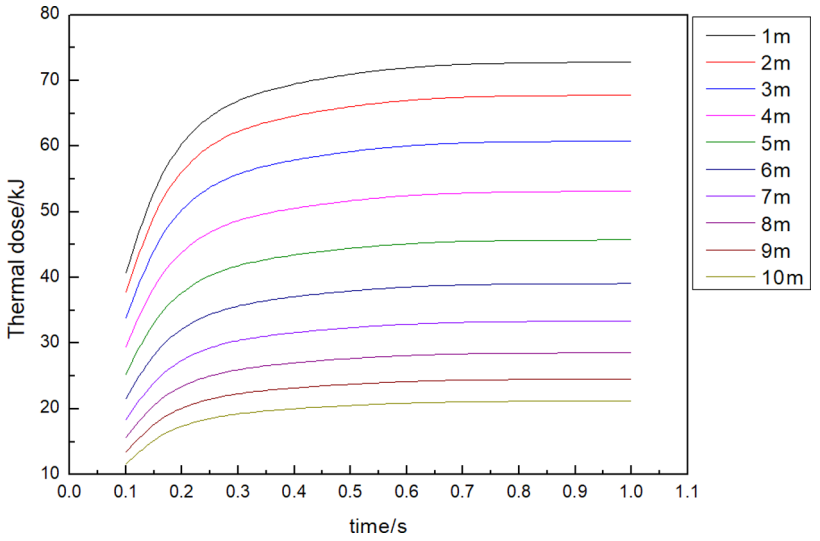

Figure 8. Dynamic curve of thermal dose at different distances by the effective band integration method.

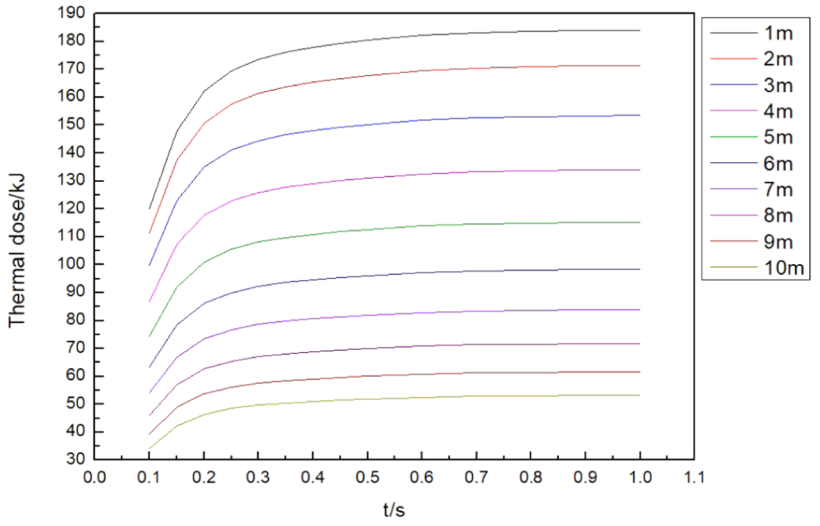

Figure 9. Dynamic change curve of thermal dose at different distances by the full-band integration method.

In this paper, the effective band integral method is used to calculate the fireball heat dose Q, which is compared with the fireball heat radiation heat dose Q_2 calculated by the Stephen–Boltzmann formula of the full-band method. During the effective time of the fireball, the different test distances are compared and analyzed. The calculated results of the final heat dose received by the target are shown in Table 4.

In addition, to observe the dynamic change process of fireball heat dose more intuitively and clearly, Figures 8 and 9 show the dynamic change curve of fireball heat dose received by targets at different distances over time.

Analyzing the dynamic change curve of thermal dose, it is found that as the test distance increases, the thermal dose of the fireball gradually decreases; with the increase of time, the accumulated thermal dose at the same distance gradually increases, but the increase is smaller and smaller. The thermal dose Q calculated by the effective band integration method used in this paper is 72.81 kJ·m^{-2} at the maximum, and the corresponding damage level is skin pain, and the fireball thermal dose Q_2 calculated by the full-band integration method is the smallest at 53.23 kJ·m^{-2}, the damage level is skin pain. Q_2 at any distance is generally larger than the Q calculated by the effective band integration method in this paper. On the whole, Q_2 calculated at any distance is more than 2.5 times that of Q.

5. CONCLUSIONS

To more accurately evaluate the thermal damage performance of the ammunition, this paper proposes to calculate the radiant energy of the fireball surface based on the effective band integral method and establishes a dynamic model of the fireball's thermal radiation dose Q. The following conclusions can be drawn:

According to the 30 kg thermobaric explosive fireball data measured by the infrared thermal imager, the equivalent average temperature, the diameter of the fireball, and the height of the center of the fireball on the surface of the thermobaric explosive fireball are fitted to establish the dynamic relationship with time, which can more accurately and effectively reveal the changing laws of the fireball.

The analysis of the existing test results found that the temperature distribution at each point on the surface of the fireball is not uniform. According to the principle of radiation temperature measurement, the average temperature Ta of the

https://doi.org/10.1021/acsomega.3c03980
ACS Omega 2023, 8, 29717−29724

equivalent thermal radiation intensity is used to represent the surface temperature of the fireball.

On the basis of Planck's black body radiation theorem, the Stephen−Boltzmann formula is improved, and the energy of the fireball surface radiation is obtained by integrating with the effective wavelength band of the infrared thermal imager. The target is calibrated by the on-site temperature to obtain the on-site atmospheric transmittance, compared with the full-band integration method, which can more accurately assess the heating damage effect of the fireball.

AUTHOR INFORMATION

Corresponding Authors

Pan Pei − *State Key Laboratory of Dynamic Measurement Technology, North University of China, Taiyuan 030051 Shanxi, China*; orcid.org/0000-0002-6677-0409; Email: 1370974208@qq.com

Hongmian Du − *State Key Laboratory of Dynamic Measurement Technology, North University of China, Taiyuan 030051 Shanxi, China*; Email: duhongmian@nuc.edu.cn

Author

Xiaojian Hao − *State Key Laboratory of Dynamic Measurement Technology, North University of China, Taiyuan 030051 Shanxi, China*

Complete contact information is available at: https://pubs.acs.org/10.1021/acsomega.3c03980

Notes

The authors declare no competing financial interest.

ACKNOWLEDGMENTS

This study was financially supported by the Fund of National Natural Science Fund (no. 52075504), the Fund for Shanxi "1331Project" Key Subject Construction, the Shanxi Postgraduate Education Innovation Program (no. 2022Y584), and the Fund for State Key Laboratory of Quantum Optics and Quantum Optics Devices (no. KF202301). The authors thank all of the reviewers, editors, and contributors for their contributions and suggestions.

REFERENCES

(1) Guo, X. Y.; Li, B.; Li, F.; et al. Study on Thermal Damage of Thermobaric Explosive. *Chin. J. Propellants* **2008**, *31*, 16−19.

(2) Liu, X.; Hao, X.; Xue, B.; Tai, B.; Zhou, H.; et al. Two-Dimensional Flame Temperature and Emissivity Distribution Measurement Based on Element Doping and Energy Spectrum Analysis. *IEEE Access* **2020**, *8*, 63−74.

(3) Bing, X.; Xiaojian, H.; Xuanda, L.; Ziqi, H.; Hanchang, Z.; et al. Simulation of an NSGA-III Based Fireball Inner-Temperature-Field Reconstructive Method. *IEEE Access* **2020**, *8*, 43908−43919.

(4) He, Z. G. *Research on Thermal Radiation Effect of FAE Explosion Fireball*; Nanjing University of Science and Technology: Nanjing, 2004; pp 29−35.

(5) Li, B.; Guo, X. Y.; Xie, L. F. Study on Thermal Sustaining Damage Ability of Thermobaric Explosive. *J Ballist* **2009**, *21*, 99−102.

(6) Baker, W. E.; Cox, P. A.; Westine, P. S.et al. *Explosion Hazards and Evaluation[M]// Explosion Hazards and Evaluation*; Elsevier Scientific Pub. Co.: Amsterdam, 1983.

(7) Yu, D. M.; Feng, C. G.; Xu, Z. S.; et al. Injury effects of shock waves, heat radiation and house collapse in explosive explosion accidents. *Acta Armamentarii* **1998**, *19*, 33−37.

(8) Li, X. L. *Research on Related Technologies of Thermo-Pressure Agent Based on Combustion and Explosion Effects*; Nanjing University of Science and Technology: Nanjing, 2008; pp 100−103 (in Chinese).

(9) Zhong, Q.; Wang, B. L.; Huang, J.; et al. Application of a dynamic model to thermal damage estimation of thermobaric explosives. *Explos. Shock Waves* **2011**, *31*, 528−532.

(10) Wang, Y.-x.; Liu, Y.; Xu, Q.-m.; Li, B.; Xie, L.-f.; et al. Effect of metal powders on explosion of fuel-air explosives with delayed secondary igniters. *Def. Technol.* **2021**, *17*, 785−791.

(11) Zhong, Q.; Liu, D. B.; Qiu, S. S.; et al. Temperature Measurement Study on Blasting Fireball of Thermobaric Explosives. *Explos. Mater.* **2019**, *48*, 23−26,31.

(12) Kan, J. L. *Research on Explosion and Damage Characteristics of Liquid-solid Composite Cloud Explosive Agent*; Nanjing University of Science and Technology: Nanjing, 2008; pp 42−46.

(13) Xu, X. Z.; Pei, J. M.; Wang, Y. H.; et al. Dispersion Characteristics of Single-event FAE. *Chin. J. Explos. Propellants* **2000**, *23*, 47−49, 46.

(14) Martinsen, W. E.; Marx, J. D. In *An Improved Model for the Prediction of Radiant Heat from Fireballs*; International Conference and Workshop on Modeling the Consequences of Accidental Releases of Hazardous Materials, CCPS: San Francisco, California, 1999; pp 605−621.

(15) Skrinska, M.; Skrinsky, J.; Sluka, V.; et al. Mathematical Models for the Prediction of Heat Flux from Fire Balls. *WSEAS Transactions on Heat and Mass Transfer* **2014**, *9*, 243−250.

(16) Zhang, D. L.; Liu, M.; Wang, W.; et al. On the dynamic model application to the fireball radiation consequence calculation. *J. Saf. Environ.* **2007**, *7*, 132−135.

(17) Xu, G. Z.; Zhang, L.; Zhang, X. G.; et al. A Review on Burning Damage Technology. *Chin. J. Energy Mater.* **2021**, *29*, 667−679.

(18) Yang, Y.; Hao, X.; Zhang, L.; Ren, L.; et al. Application of Scikit and Keras Libraries for the Classification of Iron Ore Data Acquired by Laser-Induced Breakdown Spectroscopy (LIBS). *Sensor* **2020**, *20*, No. 1393.

(19) Zhang, Z. Q.; Wang, P.; Yu, X. D.; et al. Study on high accuracy temperature measurement technology of infrared thermal imager. *Chin. J. Sci. Instrum.* **2020**, *41*, 10−18.

(20) Wang, L.-Y.; Du, H.-M.; Xu, H. Compensation method for infrared temperature measurement of explosive fireball. *Thermochim. Acta* **2019**, *680*, No. 178342.

(21) Wang, W.; Du, H. M.; Fan, J. B.; et al. Measurement and calculation technology of temperature compensation of explosion flame based on infrared radiation. *Explos. Shock Waves* **2021**, *41*, No. 054101.

(22) An, W. S.; Lu, W.; Li, H. X.; et al. Assessment of Damage in Heat Radiation of Incendiary Bomb on Q Criterion. *J. Ordnance Equip. Eng.* **2019**, *40*, 95−97, 136.